N^6-methyladenosine modification and the YTHDF2 reader protein play cell type specific roles in lytic viral gene expression during Kaposi's sarcoma-associated herpesvirus infection

Charles Hesser[1], John Karijolich[2,3], Dan Dominissini[4,5,6], Chuan He[4,7], and Britt Glaunsinger[1,2,7]

[1]Department of Molecular and Cell Biology, [2]Department of Plant & Microbial Biology, University of California Berkeley; [3]Department of Pathology, Microbiology, and Immunology, Vanderbilt University Medical Center, Nashville, TN 37232-2363, [4]Department of Chemistry, Department of Biochemistry and Molecular Biology, and Institute for Biophysical Dynamics, The University of Chicago, Chicago, Illinois, USA; [5]Chaim Sheba Medical Center, Tel Hashomer 52621, Israel; [6]Sackler School of Medicine, Tel Aviv University, Tel Aviv, Israel, [7]Howard Hughes Medical Institute

*Corresponding author: glaunsinger@berkeley.edu

17

18 **Abstract**

19 Methylation at the N^6 position of adenosine (m^6A) is a highly prevalent and reversible
20 modification within eukaryotic mRNAs that has been linked to many stages of RNA processing
21 and fate. Recent studies suggest that m^6A deposition and proteins involved in the m^6A pathway
22 play a diverse set of roles in either restricting or modulating the lifecycles of select viruses.
23 Here, we report that m^6A levels are significantly increased in cells infected with the oncogenic
24 human DNA virus Kaposi's sarcoma-associated herpesvirus (KSHV). Transcriptome-wide m^6A-
25 sequencing of the KSHV-positive renal carcinoma cell line iSLK.219 during lytic reactivation
26 revealed the presence of m^6A across multiple kinetic classes of viral transcripts, and a
27 concomitant decrease in m^6A levels across much of the host transcriptome. However, we found
28 that depletion of the m^6A machinery had differential pro- and anti-viral impacts on viral gene
29 expression depending on the cell-type analyzed. In iSLK.219 cells the pathway functioned in a
30 pro-viral manner, as depletion of the m^6A writer METTL3 and the reader YTHDF2 significantly
31 impaired viral lytic cycle progression and virion production. This defect could be attributed to
32 their roles in the post-transcriptional accumulation of the major viral lytic transactivator ORF50,
33 which is m^6A modified. In contrast, although the ORF50 mRNA was also m^6A modified in KSHV
34 infected B cells, ORF50 expression was instead increased upon depletion of METTL3, YTHDF1,
35 or, to a lesser extent, YTHDF2. These results highlight that the m^6A pathway is centrally
36 involved in regulating KSHV gene expression, and underscore how the outcome of this
37 dynamically regulated modification can vary significantly between cell types.

38

39 **Author Summary**

40 In addition to its roles in regulating cellular RNA fate, methylation at the N^6 position of
41 adenosine (m^6A) of mRNA has recently emerged as a mechanism for regulating viral infection.
42 While it has been known for over 40 years that the mRNA of nuclear replicating DNA viruses
43 contain m^6A, only recently have studies began to examine the distribution of this modification
44 across viral transcripts, as well as characterize its functional impact upon viral lifecycles. Here,
45 we apply m^6A-sequencing to map the location of m^6A modifications throughout the
46 transcriptome of the oncogenic human DNA virus Kaposi's sarcoma-associated herpesvirus
47 (KSHV). We show that the m^6A machinery functions in a cell type specific manner to either
48 promote or inhibit KSHV gene expression. Thus, the KSHV lifecycle is impacted by the m^6A
49 pathway, but the functional outcome may depend on cell lineage specific differences in m^6A-
50 based regulation.

51

52 **Introduction**

53 The addition of chemical modifications is critical to many steps of mRNA processing and
54 the regulation of mRNA fate. There are more than 100 different RNA modifications, but the
55 most abundant internal modification of eukaryotic mRNAs is N^6-methyladenosine (m^6A), which
56 impacts nearly every stage of the posttranscriptional mRNA lifecycle from splicing through
57 translation and decay [1-6]. The breadth of impacts ascribed to the m^6A mark can be attributed
58 to its creation of new platforms for protein recognition, in part via local changes to the RNA

59 structure [4,7-12]. The reversibility of m^6A deposition through the activity of demethylases
60 termed erasers adds a further layer of complexity by enabling dynamic regulation, for example
61 during developmental transitions and stress [1,4,5,13-15]. Deposition of m^6A occurs co- or post-
62 transcriptionally through a complex of proteins with methyltransferase activity known as
63 writers, which include the catalytic subunit METTL3 and cofactors such as Mettl14 and WTAP
64 [1,4,14,16,17]. The modification is then functionally 'interpreted' through the selective binding
65 of m^6A reader proteins, whose interactions with the mRNA promote distinct fates.

66 The best-characterized m^6A readers are the YTH domain proteins. The nuclear YTHDC1
67 reader promotes exon inclusion [6], whereupon m^6A-containing mRNA fate is guided in the
68 cytoplasm by the YTHDF1-3 readers. Generally speaking, YTHDF1 directs mRNAs with 3' UTR
69 m^6A modifications to promote translation [3], whereas YTHDF2 recruits the CCR4-NOT
70 deadenylase complex to promote mRNA decay [18]. YTHDF3 has been proposed to serve as a
71 co-factor to potentiate the effects of YTHDF1 and 2 [3,19,20]. Although the individual effects of
72 YTHDF1 and 2 seem opposing, the YTHDF proteins may coordinate to promote accelerated
73 mRNA processing during developmental transitions and cellular stress [1]. YTHDC2, the fifth
74 member of the YTH family proteins, was recently shown to play critical roles in mammalian
75 spermatogenesis through regulating translation efficiency of target transcripts [21]. Additional
76 examples of distinct functions for m^6A readers under specific contexts such as heat shock are
77 rapidly emerging [13].

78 Given the prevalence of the m^6A modification on cellular mRNAs, it is not surprising that
79 a number of viruses have been shown to contain m^6A in their RNA [22-29]. Indeed, a potential
80 viral benefit could be a less robust innate antiviral immune response, as m^6A modification of in

81 vitro synthesized RNAs diminishes recognition by immune sensors such as TLR3 and RIG-I
82 [30,31]. That said, the functional consequences of viral mRNA modification appear diverse and
83 include both pro- and anti-viral roles. In the case of Influenza A, a negative sense ssRNA virus,
84 m^6A and the reader YTHDF2 have been shown to promote viral replication [32]. Furthermore,
85 multiple studies have mapped the sites of m^6A modification in the human immunodeficiency
86 virus (HIV) genome, and shown that it promotes the nuclear export of HIV mRNA as well as viral
87 protein synthesis and RNA replication [24,26,28]. Roles for the YTHDF proteins in during HIV
88 infection remain varied however, as Tirumuru and colleagues propose they function in an anti-
89 viral context by binding viral RNA and inhibiting reverse transcription, while Kennedy and
90 colleagues observe they enhance HIV replication and viral titers [24,28]. A more consistently
91 anti-viral role for the m^6A pathway has been described for the *Flaviviridae*, whose (+) RNA
92 genomes are replicated exclusively in the cytoplasm and contain multiple m^6A sites in their
93 genomic RNA [23,25]. An elegant study by Horner and colleagues showed that depletion of
94 m^6A writers and readers or the introduction of m^6A-abrogating mutations in the viral E1 gene
95 all selectively inhibit hepatitis C virus (HCV) assembly [23]. Similarly, depletion of METTL3 or
96 Mettl14 enhances Zika virion production [25].

97 Despite the fact that m^6A modification of DNA viruses was first reported more than 40
98 years ago for simian virus 40, herpes simplex virus type 1, and adenovirus type 2, roles for the
99 modification in these and other DNA viruses remain largely unexplored [33-37]. Unlike most
100 RNA viruses, with few exceptions DNA viruses replicate in the nucleus and rely on the cellular
101 transcription and RNA processing machinery, indicating their gene expression strategies are
102 likely interwoven with the m^6A pathway. Indeed, it was recently shown that the nuclear reader

103 YTHDC1 potentiates viral mRNA splicing during lytic infection with Kaposi's sarcoma-associated
104 herpesvirus (KSHV) [38]. However, roles for the cytoplasmic m^6A readers during DNA virus
105 infection, as well as a transcriptome-level understanding of how DNA viruses incorporate m^6A
106 and influence the spectrum of m^6A deposition on cellular mRNAs remain key open questions.

107 Here, we sought to address these questions by measuring and mapping the abundance
108 of m^6A marks across the viral and host transcriptome during lytic KSHV infection. This
109 gammaherpesvirus remains the leading etiologic agent of cancer in AIDS patients, in addition to
110 causing the lymphoproliferative disorders multicentric Castleman's disease and primary
111 effusion lymphoma. The default state for KSHV in cultured cells is latency, although in select
112 cell types the virus can be reactivated to engage in lytic replication, which involves a temporally
113 ordered cascade of gene expression. We reveal that m^6A levels are significantly increased upon
114 KSHV reactivation, which is due to a combination of m^6A deposition across multiple kinetic
115 classes of viral transcripts and a concomitant decrease in m^6A levels across much of the host
116 transcriptome. Depletion of m^6A writer and cytoplasmic reader proteins either moderately or
117 severely impaired viral lytic cycle progression in the KSHV iSLK.129 reactivation model,
118 suggesting this pathway potentiates the KSHV lytic cycle. Interestingly, however, the roles for
119 the m^6A writer and readers shifted to instead display neutral or anti-viral activity in the TREX-
120 BCBL1 reactivation model. These findings thus demonstrate that while KSHV mRNAs are
121 marked by m^6A, the functional consequences of this mark can vary significantly depending on
122 cell context, reinforcing both the functional complexity and dynamic influence of m^6A.

123

124 **Results**

125 **KSHV mRNA contains m^6A modifications**

126 Epitranscriptome mapping has revealed significant roles for the m^6A pathway in the
127 lifecycle and regulation of several RNA viruses, but similar global analyses have yet to be
128 performed for a DNA virus. Given that herpesviral mRNAs are transcribed and processed in the
129 nucleus using the cellular RNA biogenesis machinery, we hypothesized that these viruses would
130 engage the m^6A pathway. We therefore first quantified how KSHV reactivation impacted total
131 cellular m^6A levels in the KSHV-positive renal carcinoma cell line iSLK.219 (**Fig 1**). These cells are
132 a widely used model for studying viral lytic events, as they stably express the KSHV genome in a
133 tightly latent state but harbor a doxycycline (dox)-inducible version of the major viral lytic
134 transactivator ORF50 (also known as RTA) that enables efficient entry into the lytic cycle
135 [39,40]. Polyadenylated (polyA+) RNA was enriched from untreated (latent) or dox-reactivated
136 iSLK.219 cells and the levels of m^6A were quantitatively analyzed by liquid chromatography-
137 tandem mass spectrometry (LC-MS/MS) (**Fig 1A**). Indeed, we observed a three-fold increase in
138 total m^6A levels upon KSHV lytic reactivation, suggesting that m^6A deposition significantly
139 increased during viral replication (**Fig 1B**).

140 We next sought to discern whether the increase in m^6A during the KSHV lytic cycle
141 favors host or viral mRNAs using high throughput m^6A RNA sequencing (m^6Aseq) [41]. This
142 technique can reveal both the relative abundance and general location of m^6A in KSHV and
143 cellular mRNA. Total m^6A containing RNA was immunoprecipitated from 2 biological replicates
144 of latent or lytically reactivated iSLK.219 cells using an m^6A-specific antibody. DNase-treated

145 total mRNA was fragmented to lengths of 100 nt prior to immunoprecipitation and then
146 subjected to m^6A-seq. Total RNA-seq was run in parallel for each sample, allowing the degree
147 of m^6A modification to be normalized with respect to transcript abundance because the levels
148 of many transcripts change upon viral lytic reactivation. Peaks with a fold-change four or higher
149 (FC>4) and a false discovery rate of 5% or lower (FDR>5%) in both replicates were considered
150 significant, although it is possible that additional transcripts detectably modified to lower levels
151 or in a more dynamic manner may also be functionally regulated by m^6A (complete list of viral
152 peaks with FC>2 in **S1 Table**). In lytically reactivated samples, 10 transcripts comprising genes of
153 immediate early, early, and late kinetic classes displayed significant m^6A modification in both
154 replicates (**Fig 2A** and **S1 Fig**). Within these KSHV mRNAs, m^6A peaks were detected primarily in
155 coding regions, although in some cases the location of a peak in a coding region overlaps with a
156 UTR (**S1 Fig)**. Furthermore, all but one peak contains at least one instance of the GG(m^6A)C
157 consensus sequence. While many of the modified viral transcripts contained only one m^6A
158 peak, multiple peaks were found in certain transcripts, including the major lytic transactivator
159 ORF50 (**Fig 2B**). Of note, exon2 of ORF50 contained one m^6A peak of FC>4 in replicate one, and
160 three m^6A peaks in replicate two, each of which have at least one m^6A consensus motif, further
161 increasing confidence that these peaks accurately represent m^6A modified sites. Furthermore,
162 the viral ncRNA PAN, which has been reported to comprise over 80% of nuclear PolyA+ RNA
163 during lytic reactivation [42], contains FC>4 peaks in both replicates. Modification of PAN likely
164 accounts for the marked three-fold increase in cellular m^6A content observed upon lytic
165 reactivation (Fig 1B). As anticipated given the restricted viral gene expression profile during
166 latency, unreactivated samples had many fewer m^6A containing viral mRNAs, with the only

167 FC>4 peaks occurring in both replicates located in ORF4. Although ORF4 is a lytic transcript, its
168 coding region overlaps with the 3' UTR of K1, which is expressed during both the latent and lytic
169 phases of the viral lifecycle (**Fig 2A**, **S1 Fig**) [43,44].

170 To validate the m^6A-seq results, we performed m^6A RNA immunoprecipitation (RIP)
171 followed by quantitative real-time PCR (RT-qPCR) on six of the viral transcripts predicted to be
172 m^6A modified from the m^6A-seq data. This technique allows determination of the relative level
173 of m^6A content in a given transcript compared to an unmodified transcript. As controls, we
174 included primers for the cellular GAPDH transcript, which is known not to be m^6A modified, and
175 the Dicer transcript, which is m^6A modified [41]. The m^6A RIP RT-qPCR confirmed modification
176 of the vIL-6, K1, ORF50, ORF57 and PAN viral transcripts, in agreement with m^6A-seq results (**Fig**
177 **2C**). In summary, we found m^6A modification in approximately one third of KSHV transcripts
178 upon lytic reactivation, consistent with the hypothesis that this pathway contributes to KSHV
179 gene expression.

180 We next compared the distribution of m^6A peaks in host mRNAs from unreactivated
181 versus reactivated cells to assess whether lytic KSHV infection altered the m^6A profile of cellular
182 transcripts. Analyzing the two independent replicates for each condition, we found an average
183 of 14,092 m^6A modification sites (FC>4 and FDR>5%) in host transcripts pre-reactivation,
184 compared to 10,537 peaks post-reactivation (**Fig 2D** and **S2 Table**). We observed that this >25%
185 decrease in m^6A deposition on cellular mRNA encompassed a wide spectrum of transcripts, and
186 no notable patterns were apparent by GO term analysis for functional categories enriched in
187 the altered population. Thus, while the functional impact of the altered host m^6A profile
188 remains unresolved, the observation that KSHV lytic infection increased the level of m^6A in total

189 poly A+ RNA despite decreasing its presence in cellular mRNA implies that m^6A deposition
190 during infection favors viral transcripts.

191

192 **m^6A and the reader YTHDF2 mediate viral gene expression and virion production in iSLK.219**
193 **cells**

194 Given the significant deposition of m^6A across KSHV transcripts, we reasoned that m^6A
195 might play an important role in potentiating the viral lifecycle. We therefore examined the
196 effect of depleting the m^6A writers and readers on KSHV virion production using a supernatant
197 transfer assay. The KSHV genome in iSLK.219 cells contains a constitutively expressed version
198 of GFP, which allows for fluorescence-based monitoring of infection by progeny virions. We
199 performed siRNA-mediated knockdown of METTL3, the catalytic subunit responsible for m^6A
200 deposition, as well as the m^6A readers YTHDF 1, 2 and 3 (**Fig 3A**). Cells were then treated with
201 dox and sodium butyrate to induce lytic reactivation for 72 h, whereupon supernatants were
202 collected and used to infect 293T recipient cells. The number of GFP positive 293T cells at 24
203 hpi was measured by flow cytometry (**Fig 3B**). Notably, for virus generated from METTL3
204 depleted cells, only 7% of recipient cells were infected compared to 82% for virus generated
205 during treatment with a control siRNA (**Fig 3B**). YTHDF2 depletion caused an even more
206 pronounced defect, resulting in a near absence of virion production. In contrast, YTHDF3
207 knockdown resulted in only a modest defect and virion production was unaffected by YTHDF1
208 knockdown (**Fig 3B**). Thus, the m^6A writer METTL3 and the reader YTHDF2 play important roles
209 in driving KSHV infectious virion production in iSLK.219 cells.

210 We then sought to determine the stage of the viral lifecycle impacted by the m^6A
211 pathway by measuring the impact of writer and reader depletion on the abundance of viral
212 mRNAs of different kinetic classes. First, levels of representative immediate early, delayed
213 early, and late viral mRNAs were measured by RT-qPCR following lytic reactivation for 72 hours.
214 Of note, all of these transcripts contained at least one m^6A peak. METTL3 depletion did not
215 appear to impact accumulation of the ORF50 immediate early mRNA at this time point, but
216 resulted in a significant defect in accumulation of the delayed early transcript ORF57 and late
217 gene transcript K8.1 (**Fig 3C**). Consistent with the virion production data, we observed a striking
218 defect in the accumulation of each of the viral transcripts upon YTHDF2 depletion, suggesting
219 that this protein is essential for lytic KSHV gene expression beginning at the immediate early
220 stage (**Fig 3C**). In contrast, viral gene expression was either unaltered or modestly increased
221 upon depletion of YTHDF1 or YTHDF3 (**Fig 3C**). These results for ORF50 and ORF59 were
222 confirmed at the protein level by Western blot, showing that depletion of YTHDF2 but not the
223 other m^6A pathway components resulted in a near total inhibition of viral protein expression at
224 this late stage in the viral lifecycle (**Fig 3D**). We noted that although depletion of METTL3 did
225 not significantly decrease the level of ORF50 mRNA, levels of METTL3 knockdown in excess of
226 80% have only been reported to reduce m^6A levels in Poly A RNA by 20-30% [17]. Thus, at least
227 some fraction of ORF50 (and other) transcripts may still be m^6A modified due to residual
228 enzyme activity upon depletion of METTL3.

229 In agreement with the above findings, we also observed that iSLK.219 cells depleted of
230 METTL3 and YTHDF2 displayed a prominent defect in viral reactivation, as measured by
231 expression of red fluorescent protein (RFP) driven by the PAN lytic cycle promoter from the

232 viral genome (**Fig 3E**). Similarly, ORF50 protein production was also markedly reduced upon
233 YTHDF2 depletion at the 24 h time point, which represents the early phase of the lytic cycle for
234 cells reactivated with dox alone (**Fig 3F**). Collectively, these results suggest that m^6A
235 modification is integral to the KSHV lifecycle, and that YTHDF2 plays a particularly prominent
236 role in mediating KSHV lytic gene expression in iSLK.219 cells.

237

238 **The m^6A pathway post-transcriptionally controls ORF50 expression in iSLK.219 cells**

239 ORF50 is the major viral transcriptional transactivator, and its expression is essential to
240 drive the KSHV lytic gene expression cascade [45]. The observations that ORF50 is m^6A
241 modified and that its accumulation is dependent on YTHDF2 indicate that the m^6A pathway
242 plays key roles in ORF50 mRNA biogenesis or fate in iSLK.219 cells, potentially explaining the
243 lytic cycle progression defect in the knockdown cells. m^6A deposition has been reported to
244 occur both co-transcriptionally and post-transcriptionally [1,16,17,46] . To determine whether
245 the m^6A pathway is important for ORF50 synthesis or mRNA turnover, we measured its
246 transcription in reactivated iSLK.219 cells upon depletion of METTL3, YTHDF1, 2, or 3 using 4-
247 thiouridine (4sU) metabolic pulse labeling. 4sU is a uridine derivative that can be used to
248 isolate newly transcribed RNA, as thiol-specific biotinylation of the 4sU-containing RNA enables
249 its purification over streptavidin-coated beads [47,48]. At 24 h post reactivation, the siRNA
250 treated iSLK.219 cells were pulse labeled with 4sU for 30 min, whereupon the labeled nascent
251 RNA was isolated by biotin-streptavidin purification and viral transcripts were quantified by RT-
252 qPCR (**Fig 4A)**. Despite the defect in ORF50 accumulation observed upon YTHDF2 depletion

253 (see **Fig 3A**), we observed no decrease in ORF50 transcription upon depletion of any of the m^6A
254 writer or reader proteins (**Fig 4B**). However, in YTHDF2 depleted cells, there was a prominent
255 defect in the transcription of ORF37, likely because transcription of delayed early and late viral
256 genes is dependent on the presence of ORF50 protein (**Fig 4C**).

257 The observation that YTHDF2 was important for mediating the post-transcriptional,
258 stable accumulation of ORF50 mRNA suggested that the transcriptional context of ORF50
259 should not impact its regulation by the m^6A pathway in iSLK cells. Indeed, depletion of METTL3
260 or YTHDF2 also reduced the accumulation of ORF50 protein in an uninfected iSLK cell line
261 containing an integrated, dox-inducible ORF50 gene (iSLK.puro cells) (**Fig 4D and 4E**). Here,
262 YTHDF3 depletion resulted in an increase in ORF50 expression, which we also observed to a
263 more modest degree in the iSLK.219 cells (see **Fig 3D**). Overall, these data suggest that YTHDF2
264 depletion causes post-transcriptional degradation of the ORF50 mRNA, leading to a block in
265 KSHV lytic cycle progression in infected iSLK.219 cells.

266

267 **The impact of m^6A on KSHV infection is cell type specific**

268 Finally, given the diversity of functions reported for m^6A in controlling cellular processes and
269 RNA virus infections [1,22,27], we sought to evaluate the role of this pathway in another widely
270 used KSHV infected cell line of distinct origin, the B cell line TREX-BCBL1 [49]. Similar to
271 iSLK.219 cells, TREX-BCBL1 cells also contain a dox-inducible copy of ORF50 to boost
272 reactivation. The m^6A pathway components were depleted from TREX-BCBL1 cells via siRNA
273 treatment, whereupon cells were reactivated for 72 hr with dox, TPA, and ionomycin and the

274 abundance of the ORF50 and ORF59 lytic cycle proteins was monitored by western blot.
275 Consistent with observations in iSLK.219 cells, ORF50 and ORF59 expression was not affected
276 by depletion of YTHDF3, although it was enhanced by depletion of YTHDF1 (**Fig 5A and 5B**).
277 However, knockdown of METTL3 and YTHDF2 resulted in phenotypes clearly distinct from those
278 observed in iSLK.219 cells. There was a marked increase in ORF50 expression in METTL3
279 depleted TREX-BCBL1 cells, and near or above WT levels of ORF50 and ORF59 upon YTHDF2
280 knockdown (**Fig 5B**). We next examined whether the ORF50 mRNA was subject to m^6A
281 modification in reactivated TREX-BCBL1 cells by m^6A RIP, followed by RT-qPCR using control or
282 ORF50 specific primers. Indeed, there was a clear enrichment of ORF50 in the reactivated,
283 m^6A-containing RNA population (**Fig 5C**). As expected, we detected the m^6A modified DICER
284 transcript in both reactivated and unreactivated cells, whereas the unmodified GAPDH
285 transcript was present in neither sample (**Fig 5C**). Thus, although it is possible that the
286 modification state of some viral mRNAs differs between iSLK.219 and TREX-BCBL1 cells, the
287 ORF50 transcript is modified in both cell types.

288 Finally, to determine whether these differences in the contribution of the m^6A writer
289 and readers impacted the outcome of the viral lifecycle, we measured the impact of METTL3
290 and YTHDF1-3 protein knockdown on virion production using a supernatant transfer assay.
291 TREX-BCBL1 cells lack the viral GFP marker, and thus infection of recipient cells was instead
292 measured by RT-qPCR for the KSHV latency-associated LANA transcript. Consistent with the
293 viral protein expression data from METTL3 or YTHDF2-depleted TREX-BCBL1 cells, we observed
294 a modest, though not statistically significant, increase in the levels of LANA mRNA in the 293T
295 recipient cells infected with these supernatants (**Fig 5D**). These data confirm that METTL3 and

296 YTHDF2 are not required for virion production in TREX-BCBL1 cells, and suggest they may
297 instead decrease the efficiency of viral amplification. In summary, while there are some
298 similarities in the impact of YTHDF1 and YTHDF3 in iSLK.219 and TREX-BCBL1 cells, METTL3 and
299 YTHDF2 appear to function in a pro-viral capacity in iSLK.219 cells but in an antiviral capacity in
300 TREX-BCBL1 cells. These findings highlight how at least a subset of m^6A pathway functions and
301 targets may diverge between cell types.

302

303 **Discussion**

304 Although m^6A modification of viral RNAs has been recognized for more than 40 years,
305 only recently are the contributions of this epitranscriptomic mark towards viral life cycles
306 beginning to be revealed. Thus far, global epitranscriptomic analyses have documented m^6A
307 deposition during infections with HIV, Influenza A virus and several members of the *Flaviviridae*,
308 with a diverse set of resulting pro- and anti-viral roles [23-26,28,32]. The breadth and
309 occasionally apparently contrasting functions for the m^6A pathway during infection are perhaps
310 unsurprising given the dynamic role for this modification in controlling mRNA fate and its ability
311 to impact virtually every stage of host gene expression [1,27]. Here, we provide the first global
312 analysis of the m^6A epitranscriptome during lytic infection with a DNA virus, KSHV, revealing the
313 presence of m^6A across multiple kinetic classes of viral transcripts and a general decrease in
314 m^6A deposition on cellular mRNAs. In the widely used KSHV-positive cell line iSLK.219, we
315 found that depletion of several components of the m^6A pathway inhibited the KSHV lytic cycle,
316 most notably by restricting the post-transcriptional accumulation of the viral lytic transactivator

317 ORF50. The YTHDF2 reader protein proved particularly important, as its depletion eliminated
318 lytic entry and virion production. These observations are suggestive of a pro-viral role for m^6A
319 in the iSLK.219 KSHV reactivation model. However, m^6A marks on mRNA in a cell are
320 widespread and contribute to a large variety of cellular and pathogenic processes that likely
321 occur in a cell type or context-dependent manner. In this regard, it is notable that a distinct set
322 of phenotypes was observed for m^6A pathway components in the B cell line TREX-BCBL1. Here,
323 YTHDF2 had little effect on ORF50 expression, whereas depletion of METTL3 or YTHDF1
324 increased ORF50 abundance, more suggestive of an anti-viral role. Thus, although KSHV
325 engages the m^6A pathway in multiple cell types, these findings underscore the importance of
326 not broadly extrapolating m^6A roles from a particular cell type, as this complex regulatory
327 pathway can functionally vary in a cell type dependent manner.

328 What might be the basis for these phenotypic differences between cell types in the
329 context of KSHV infection? While this work was in preparation, Ye and colleagues performed an
330 RT-qPCR based analysis demonstrating m^6A deposition in many KSHV mRNAs in BCBL1 cells,
331 including ORF50 [38]. We also observed ORF50 modification in TREX-BCBL1 cells. Thus, it is not
332 the case that the viral mRNAs engage the m^6A methyltransferase machinery in one cell type but
333 not the other, although it is possible that site specificity of m^6A deposition varies between cell
334 lines. The facts that m^6A deposition is dynamic and does not strictly occur on consensus motifs
335 render this possibility challenging to resolve. Indeed, how m^6A deposition selectively controls
336 gene regulation on particular transcripts or under particular stimuli remains a central
337 unanswered question in the field [1]. We hypothesize that the distinct phenotypes derive either
338 from how the viral modifications are 'interpreted' in each cell type and/or indirect effects

339 driven by an altered m^6A profile on cellular mRNAs. The recent finding that m^6A modification of
340 ORF50 in BCBL1 cells contributes to efficient splicing through binding of YTHDC1 argues that
341 modifications can have a direct cis-acting impact on KSHV mRNA fate [38]. However,
342 herpesviral mRNAs are heavily reliant on host machinery at every stage of their biogenesis.
343 Given that cellular mRNA fate is significantly altered upon depletion of METTL3 and the YTHDF
344 reader proteins [1-3,18,50], it is possible that cell type specific changes in the abundance of a
345 host factor(s) required for viral mRNA stability also contribute to the phenotypic differences.
346 Furthermore, in HIV infected cells m^6A modification and YTHDF proteins have been proposed to
347 have a combination of pro-viral and anti-viral effects, including negatively impacting reverse
348 transcription, enhancing mRNA export, and increasing viral protein production [24,26,28].
349 Therefore, the m^6A pathway might similarly facilitate distinct phenotypes at different stages of
350 the KSHV lifecycle.

351 As the 'interpreters' of m^6A marks, the individual reader proteins play prominent roles
352 in modulating gene expression. Generally speaking, in HeLa and 293T cells, YTHDF1 binding
353 correlates with increased translational efficiency, YTHDF2 binding accelerates mRNA decay, and
354 YTHDF3 may serve as a cofactor to assist the other reader protein function [1-4,19,20,50].
355 However, other roles for these factors are rapidly emerging, particularly in the context of cell
356 stress, infection, or in the control of specific transcripts [7,13,15,23-26,28,50,51]. Furthermore,
357 m^6A is enriched in certain tissues, and different m^6A patterns have been found depending on
358 the tissue and developmental stage [41,52]. Intriguingly, a recent study showed that hypoxia
359 increases global m^6A content of mRNA, with many m^6A modified RNAs exhibiting increased
360 stability, raising the possibility that m^6A deposition could also stabilize transcripts during other

361 forms of cellular stress [53]. In KSHV-infected iSLK.219 cells, YTHDF2 appears essential for the
362 post-transcriptional accumulation of ORF50, a role seemingly at odds with its more canonical
363 mRNA destabilizing function. Although less dramatic viral gene expression phenotypes were
364 observed upon Mettl3 and YTHDF1 depletion, they nonetheless were required for WT levels of
365 progeny virion production. It is perhaps notable that even though YTHDF1 depletion modestly
366 enhanced the abundance of the ORF50, ORF37, ORF57, and K8.1 mRNAs, this ultimately did not
367 lead to WT virion production. An important consideration may be that m^6A factors
368 differentially impact specific KSHV transcripts, or play different roles at distinct times during
369 infection. However, dissecting these possibilities is likely to be complicated by the changes in
370 ORF50 expression (either positive or negative), which will have ripple effects on the entire lytic
371 life cycle.

372 Another relevant question is the extent to which m^6A mediates its effects on KSHV gene
373 expression co-transcriptionally versus post-transcriptionally. A recent report indicated that m^6A
374 is primarily installed in nascent mRNA in exons and affects cytoplasmic stability, but not splicing
375 [16,46]. It has also been demonstrated that that m^6A can be installed co-transcriptionally, and
376 that slowing the rate of RNA Pol II elongation enhances m^6A modification of mRNAs in a
377 manner that ultimately decreases translation efficiency [16,46]. These add to a growing body
378 of literature indicating that the position of m^6A in a transcript is a key feature impacting the
379 functional consequence of the modification [1,3,6,7,13,20]. For example, m^6A in the 3' UTR has
380 been shown to recruit YTHDF1 and enhance translation initiation in HeLa cells, while deposition
381 of m^6A in the 5' UTR has been shown to enhance 5' cap independent translation [3,7,13].
382 Whether these position-linked effects on translation extend to viral transcripts remains to be

383 tested, although there does not appear to be a consistent enrichment in a particular region of
384 viral mRNAs for the viruses analyzed thus far. In KSHV, m^6A sites are found throughout viral
385 ORFs, some of which also overlap with untranslated regions of other viral transcripts. As KSHV
386 transcription depends on the host RNA Pol II, the speed of transcriptional elongation on viral
387 mRNAs likely impacts co-transcriptional deposition and positioning of m^6A, and thus may
388 ultimately regulate translation efficiency of a given mRNA. Thus, in the context of KSHV
389 reactivation, a wide variety of mechanisms exist through which m^6A modification could impact
390 the transcription and translation of viral mRNA. Deciphering these remains an important
391 challenge for future studies, as we are currently in the early stages of understanding how this
392 and other viruses interface with the m^6A RNA modification pathway.

393

394 **Materials and Methods**

395 **Cell culture.** The renal carcinoma cell line iSLK.puro containing a doxycycline-inducible copy of
396 ORF50, and the KSHV infected renal carcinoma cell line iSLK.219 bearing docycycline-inducible
397 ORF50 [40] were cultured in Dulbecco's modified Eagle medium (DMEM; Invitrogen) with 10%
398 fetal bovine serum (FBS; Invitrogen, HyClone) and 100 U/ml penicillin-streptomycin
399 (Invitrogen). The KSHV-positive B cell line TREX-BCBL-1 containing a doxycycline-inducible
400 version of ORF50 [49] was cultured in RPMI medium (Invitrogen) supplemented with 20% FBS,
401 100 U/ml penicillin/streptomycin, and 200 uM L-glutamine (Invitrogen). HEK293T cells (ATCC)
402 were grown in DMEM (Invitrogen) supplemented with 10% FBS. To induce lytic reactivation of
403 iSLK.219 cells, $2x10^6$ cells were plated in a 10 cm dish with 1 ug/ml doxycycline (BD Biosciences)

404 and 1 mM sodium butyrate for 72 hr. Lytic reactivation of TREX-BCBL-1 cells was achieved by
405 treatment of $7x10^5$ cells/ml with 20 ng/ml 2-O-tetradecanoylphorbol-13-acetate (TPA, Sigma), 1
406 ug/ml doxycycline (BD Biosciences), and 500 ng/ml ionomycin (Fisher Scientific) for 72 hr
407 (western Blot blots for viral gene expression), or for 120 hr (supernatant transfer experiments).

408 **siRNA experiments.** For iSLK.219 cells, 100 pmol of siRNA was reverse transfected into $5x10^5$
409 cells plated in a 6-well dish using Lipofectamine RNAimax (Life Technologies). 24 hours post
410 transfection, cells were trypsinized and re-seeded on a 10 cm plate. The next day, a second
411 transfection was performed with 400 pmol siRNA and $2x10^6$ cells using the same method. The
412 following day, cells were lytically reactivated in a 10 cm plate. 24 hours post-reactivation, cells
413 were lysed in RIPA buffer (10 mM Tris-Cl (pH 8.0), 1 mM EDTA, 1% Triton X-100, 0.1% sodium
414 deoxycholate, 0.1% SDS, 140 mM NaCl) to evaluate knockdown efficiency.

415 For TREX-BCBL-1 cells, 200 pmol of siRNA was nucleofected into $2x10^6$ cells using Lonza
416 Cell Line Nucleofector Kit V and a Lonza Nucleofector 2b set to Program T001. After
417 nucleofection, cells were immediately resuspended in 2.2 ml of RPMI media in a 12 well plate.
418 24 hours later, 200 pmol of siRNA was added again to $2x10^6$ cells using the same protocol. 48
419 hours after the second transfection, cells were lysed in RIPA buffer and knockdown efficiency
420 was analyzed by Western Blot.

421 The following Qiagen siRNAs were used: SI00764715 and SI04279121 targeting YTHDF1,
422 SI04174534 targeting YTHDF2, SI00764778 and SI04205761 targeting YTHDF3, custom siRNA
423 targeting Mettl3 (sequence targeted: CTGCAAGTATGTTCACTATGA), Qiagen SI03650318
424 (negative control siRNA). The following Dharmacon siRNAs were used: SMARTpool siGenome

425 (M-021009-01-0005), targeting YTHDF2, and siGENOME Non-Targeting siRNA Pool #1
426 (D0012061305).

427 **Supernatant transfer assay and quantification of virion production**. Assays were performed as
428 previously described [54]. Briefly, for iSLK.219 cells, viral supernatant was collected 72 hr post-
429 reactivation, filtered, and added to uninfected HEK293T cells by spinfection (1500 rpm, 90
430 minutes at room temperature). 12 hours later, supernatant was removed and replaced with
431 fresh media, whereupon the cells were assessed for the successful transfer of the GFP-
432 containing KSHV BAC 24 hr post-infection using a BD Accuri C6 flow cytometer. Briefly, cells
433 were trypsinized, washed twice in PBS and resuspended in FACS Buffer (PBS with 1% FBS).
434 Uninfected HEK293T cells were used to define the GFP negative population. The percentage of
435 GFP expressing cells was quantified using FlowJo Software (FlowJo LLC). For virus produced in
436 TREX-BCBL-1 cells, supernatant transfers were performed as in iSLK.219 cells, except the virus
437 was transferred to HEK293T cells at 120 hr post-reactivation. To quantify virus produced in
438 TREX-BCBL-1 cells, RNA was extracted from HEK293T cells 48 hours post-supernatant transfer,
439 and viral gene expression was quantified by RT-qPCR using primers specific for LANA.

440 **Affinity purification and Western blotting**. Cell lysate was collected and analyzed as previously
441 described [54]. Briefly, iSLK.219 or TREX-BCBL-1 cells were trypsinized, washed with PBS and
442 lysed in RIPA buffer with protease inhibitors. After washing, SDS-sample buffer (indicate
443 components) was added to samples to elute bound proteins. Lysates were resolved by SDS-
444 PAGE and western blots were carried out with the following antibodies: rabbit ORF50 (gift of
445 Yoshihiro Izumiya, UC Davis), rabbit α-K8.1 (1:10000, antibody generated for this study), rabbit
446 α-ORF59 (1:10000, antibody generated for this study), rabbit α-Mettl3 (Bethyl, 1:1000), rabbit

447 α-YTHDF1 (Proteintech, 1:1000), rabbit α-YTHDF2 (Millipore, 1:1000), rabbit α-YTHDF3 (Sigma,
448 1:1000), and goat α-mouse and goat α-rabbit HRP secondary antibodies (1:5000; Southern
449 Biotech).

450 **4sU Labeling.** Following siRNA knockdown and 24 hr reactivation, iSLK.219 cells were pulse
451 labeled with DMEM containing 500 µM 4sU (Sigma) for 30 minutes, followed by PBS wash and
452 immediate isolation of total RNA with TRIzol. 4SU isolation was performed as previously
453 described [55]. 4SU isolated RNA was analyzed by RT-qPCR.

454 **RT-qPCR.** Total RNA was harvested using TRIzol following the manufacturer's protocol. Samples
455 were DNase treated using Turbo DNase (Ambion), and cDNA was synthesized from 2 ug of total
456 RNA using AMV reverse transcriptase (Promega), and used directly for quantitative PCR (qPCR)
457 analysis with the DyNAmo ColorFlash SYBR green qPCR kit (Thermo Scientific). All qPCR results
458 were normalized to 18S levels and WT or scramble control set to 1.

459 **LC-MS/MS analysis of m^6A.** Total RNA was isolated from iSLK219 cells with TRIzol reagent.
460 Dynabeads mRNA purification kit (Ambion) was used to isolate polyA(+) RNAs from 100ug of
461 total RNA according to the manufacturer. 100-200 ng of polyadenylated RNA was spiked with
462 10uM of 5-fluorouridine (Sigma) and digested by nuclease P1 (1 U) in 25 µL of buffer containing
463 25 mM NaCl and 2.5 mM $ZnCl_2$ at 42 °C for 2-4 h, followed by addition of NH_4HCO_3 (1 M, 3 µL)
464 and bacterial alkaline phosphatase (1 U) and incubation at 37 °C for 2 h. The sample was then
465 filtered (Amicon 3K cutoff spin column), and 5 µL of the flow through was analyzed by liquid
466 chromatography (LC) coupled to an Orbitrap-XL mass spectrometer (MS) equipped with an
467 electrospray ionization source (QB3 Chemistry facility).

468 **m^6A-RIP and m^6A-RIP-sequencing.** Total cellular RNA (containing KSHV RNA) was extracted and
469 purified by TRIzol and then DNAse treated with Turbo DNase (Ambion). 30 ul protein G
470 magnetic beads (Invitrogen) were blocked in 1% BSA solution for 1 hour, followed by incubation
471 with 12.5 ug affinity-purified anti-m^6A polyclonal antibody (Millipore) at 4°C for 2 hr with head-
472 over-tail rotation. 100 ug purified RNA was added to the antibody-bound beads in IP buffer
473 (150 mM NaCl, 0.1% NP-40, and 10 mM Tris-HCl [pH 7.4]) containing RNAse inhibitor and
474 protease inhibitor cocktail and incubated overnight at 4°C with head-over-tail rotation. The
475 beads were washed three times in IP buffer, and then RNA was competitively eluted with 6.7
476 mM m^6A-free nucleotide solution (Sigma Aldrich). RNA in the eluate was phenol chloroform
477 extracted and then reverse transcribed to cDNA for Real-Time qPCR analysis.
478 High-throughput sequencing of the KSHV methylome (m^6Aseq) was carried following the
479 previously published protocol [56]. In brief, 2.5 mg total cellular RNA was prepared from
480 iSLK.219 cells that were either unreactivated, or reactivated for five days with doxycycline. RNA
481 was isolated and DNAse treated as in the m^6A RIP, except the RNA was first fragmented to
482 lengths of ~100 nt prior to immunoprecipitation with anti-m^6A antibody (Synaptic Systems).
483 Immunoprecipitated RNA fragments and comparable amounts of input were subjected to first-
484 strand cDNA synthesis using the NEBNext Ultra RNA Library Prep Kit for Illumina (New England
485 Biolabs). Sequencing was carried out on Illumina HiSeq2500 according to the manufacturer's
486 instructions, using 10 pM template per sample for cluster generation, TruSeq SR Cluster kit v3
487 (Illumina), TruSeq SBS Kit v3-HS (Illumina) and TruSeq Multiplex Sequencing primer kit
488 (Illumina).A reference human transcriptome was prepared based on the University of California,
489 Santa Cruz (UCSC) and a reference KSHV transcriptome based on KSHV 2.0 annotation [57] .

490 Analysis of m^6A peaks was performed using the model-based analysis of ChIP-seq (MACS) peak-
491 calling algorithm. Peaks were considered significant if their MACS-assigned fold change was
492 greater than four and individual FDR value less than 5%. Sequencing data are available on GEO
493 repository (accession number GSE104621).

494 **Statistical Analysis:** All results are expressed as means +/- S.E.M. of experiments independently
495 repeated at least three times, except where indicated. Unpaired Student's t test was used to
496 evaluate the statistical difference between samples. Significance was evaluated with P values
497 <0.05.

498 **Acknowledgements**

499 This research was funded by NIH (http://www.nih.gov/) grants R01AI122528 to B.G. and
500 HG008688 to C.H. B.G. and C.H. are investigators of the Howard Hughes Medical Institute.

501

502 References

503

504 1. Roundtree IA, Evans ME, Pan T, He C. Dynamic RNA Modifications in Gene Expression
505 Regulation. Cell. 2017;169: 1187–1200. doi:10.1016/j.cell.2017.05.045

506 2. Wang X, Lu Z, Gomez A, Hon GC, Yue Y, Han D, et al. N(6)-methyladenosine-dependent
507 regulation of messenger RNA stability. Nature. 2013;505: 117–120.
508 doi:10.1038/nature12730

509 3. Wang X, Zhao BS, Roundtree IA, Lu Z, Han D, Ma H, et al. N(6)-methyladenosine
510 Modulates Messenger RNA Translation Efficiency. Cell. 2015;161: 1388–1399.
511 doi:10.1016/j.cell.2015.05.014

512 4. Fu Y, Dominissini D, Rechavi G, He C. Gene expression regulation mediated through

513 reversible m(6)A RNA methylation. Nat Rev Genet. 2014;15: 293–306.
514 doi:10.1038/nrg3724

515 5. Zhao BS, Wang X, Beadell AV, Lu Z, Shi H, Kuuspalu A, et al. m(6)A-dependent maternal
516 mRNA clearance facilitates zebrafish maternal-to-zygotic transition. Nature. 2017;542:
517 475–478. doi:10.1038/nature21355

518 6. Xiao W, Adhikari S, Dahal U, Chen Y-S, Hao Y-J, Sun B-F, et al. Nuclear m(6)A Reader
519 YTHDC1 Regulates mRNA Splicing. Molecular Cell. 2016;61: 507–519.
520 doi:10.1016/j.molcel.2016.01.012

521 7. Meyer KD, Patil DP, Zhou J, Zinoviev A, Skabkin MA, Elemento O, et al. 5' UTR m(6)A
522 Promotes Cap-Independent Translation. Cell. 2015;163: 999–1010.
523 doi:10.1016/j.cell.2015.10.012

524 8. Liu N, Pan T. N(6)-methyladenosine–encoded epitranscriptomics. Cell Research. 2016;23:
525 98–102. doi:10.1038/nsmb.3162

526 9. Liu N, Dai Q, Zheng G, He C, Parisien M, Pan T. N(6)-methyladenosine-dependent RNA
527 structural switches regulate RNA-protein interactions. Nature. 2015;518: 560–564.
528 doi:10.1038/nature14234

529 10. Zhou KI, Parisien M, Dai Q, Liu N, Diatchenko L, Sachleben JR, et al. N(6)-
530 Methyladenosine Modification in a Long Noncoding RNA Hairpin Predisposes Its
531 Conformation to Protein Binding. J Mol Biol. 2016;428: 822–833.
532 doi:10.1016/j.jmb.2015.08.021

533 11. Liu N, Zhou KI, Parisien M, Dai Q, Diatchenko L, Pan T. N(6)-methyladenosine alters RNA
534 structure to regulate binding of a low-complexity protein. Nucleic Acids Research.
535 2017;45: 6051–6063. doi:10.1093/nar/gkx141

536 12. Lewis CJT, Pan T, Kalsotra A. RNA modifications and structures cooperate to guide RNA-
537 protein interactions. Nat Rev Mol Cell Biol. 2017;18: 202–210. doi:10.1038/nrm.2016.163

538 13. Zhou J, Wan J, Gao X, Zhang X, Jaffrey SR, Qian S-B. Dynamic m(6)A mRNA methylation
539 directs translational control of heat shock response. Nature. 2015;526: 591–594.
540 doi:10.1038/nature15377

541 14. Meyer KD, Jaffrey SR. The dynamic epitranscriptome: N(6)-methyladenosine and gene
542 expression control. Nat Rev Mol Cell Biol. 2014;15: 313–326. doi:10.1038/nrm3785

543 15. Xiang Y, Laurent B, Hsu C-H, Nachtergaele S, Lu Z, Sheng W, et al. RNA m(6)A methylation
544 regulates the ultraviolet-induced DNA damage response. Nature. 2017;543: 573–576.
545 doi:10.1038/nature21671

546 16. Slobodin B, Han R, Calderone V, Vrielink JAFO, Loayza-Puch F, Elkon R, et al. Transcription

547 Impacts the Efficiency of mRNA Translation via Co-transcriptional N(6)-adenosine
548 Methylation. Cell. 2017;169: 326–337.e12. doi:10.1016/j.cell.2017.03.031

549 17. Liu J, Yue Y, Han D, Wang X, Fu Y, Zhang L, et al. A METTL3-METTL14 complex mediates
550 mammalian nuclear RNA N(6)-adenosine methylation. Nat Chem Biol. 2014;10: 93–95.
551 doi:10.1038/nchembio.1432

552 18. Du H, Zhao Y, He J, Zhang Y, Xi H, Liu M, et al. YTHDF2 destabilizes m(6)A-containing RNA
553 through direct recruitment of the CCR4-NOT deadenylase complex. Nat Commun.
554 2016;7: 12626. doi:10.1038/ncomms12626

555 19. Shi H, Wang X, Lu Z, Zhao BS, Ma H, Hsu PJ, et al. YTHDF3 facilitates translation and decay
556 of N(6)-methyladenosine-modified RNA. Cell Research. 2017;27: 315–328.
557 doi:10.1038/cr.2017.15

558 20. Li A, Chen Y-S, Ping X-L, Yang X, Xiao W, Yang Y, et al. Cytoplasmic m(6)A reader YTHDF3
559 promotes mRNA translation. Cell Research. 2017;27: 444–447. doi:10.1038/cr.2017.10

560 21. Hsu PJ, Zhu Y, Ma H, Guo Y, Shi X, Liu Y, et al. Ythdc2 is an N(6)-methyladenosine binding
561 protein that regulates mammalian spermatogenesis. Cell Research. 2017;27: 1115–1127.
562 doi:10.1038/cr.2017.99

563 22. Gokhale NS, Horner SM. RNA modifications go viral. PLoS Pathog. 2017;13: e1006188.
564 doi:10.1371/journal.ppat.1006188

565 23. Gokhale NS, McIntyre ABR, McFadden MJ, Roder AE, Kennedy EM, Gandara JA, et al.
566 N(6)-methyladenosine in Flaviviridae Viral RNA Genomes Regulates Infection. Cell Host
567 Microbe. 2016;20: 654–665. doi:10.1016/j.chom.2016.09.015

568 24. Kennedy EM, Bogerd HP, Kornepati AVR, Kang D, Ghoshal D, Marshall JB, et al.
569 Posttranscriptional m(6)A Editing of HIV-1 mRNAs Enhances Viral Gene Expression. Cell
570 Host Microbe. 2016;19: 675–685. doi:10.1016/j.chom.2016.04.002

571 25. Lichinchi G, Zhao BS, Wu Y, Lu Z, Qin Y, He C, et al. Dynamics of Human and Viral RNA
572 Methylation during Zika Virus Infection. Cell Host Microbe. 2016;20: 666–673.
573 doi:10.1016/j.chom.2016.10.002

574 26. Lichinchi G, Gao S, Saletore Y, Gonzalez GM, Bansal V, Wang Y, et al. Dynamics of the
575 human and viral m(6)A RNA methylomes during HIV-1 infection of T cells. Nat Microbiol.
576 2016;1: 16011. doi:10.1038/nmicrobiol.2016.11

577 27. Gonzales-van Horn SR, Sarnow P. Making the Mark: The Role of Adenosine Modifications
578 in the Life Cycle of RNA Viruses. Cell Host Microbe. 2017;21: 661–669.
579 doi:10.1016/j.chom.2017.05.008

580 28. Tirumuru N, Zhao BS, Lu W, Lu Z, He C, Wu L. N(6)-methyladenosine of HIV-1 RNA

581 regulates viral infection and HIV-1 Gag protein expression. Elife. 2016;5: 165.
582 doi:10.7554/eLife.15528

583 29. Martínez-Pérez M, Aparicio F, López-Gresa MP, Bellés JM, Sánchez-Navarro JA, Pallás V.
584 Arabidopsis m(6)A demethylase activity modulates viral infection of a plant virus and the
585 m(6)A abundance in its genomic RNAs. Proc Natl Acad Sci USA. 2017.
586 doi:10.1073/pnas.1703139114

587 30. Durbin AF, Wang C, Marcotrigiano J, Gehrke L. RNAs Containing Modified Nucleotides
588 Fail To Trigger RIG-I Conformational Changes for Innate Immune Signaling. MBio. 2016;7:
589 e00833–16. doi:10.1128/mBio.00833-16

590 31. Karikó K, Buckstein M, Ni H, Weissman D. Suppression of RNA recognition by Toll-like
591 receptors: the impact of nucleoside modification and the evolutionary origin of RNA.
592 Immunity. 2005;23: 165–175. doi:10.1016/j.immuni.2005.06.008

593 32. Courtney DG, Kennedy EM, Dumm RE, Bogerd HP, Tsai K, Heaton NS, et al.
594 Epitranscriptomic Enhancement of Influenza A Virus Gene Expression and Replication.
595 Cell Host Microbe. 2017;22: 377–386.e5. doi:10.1016/j.chom.2017.08.004

596 33. Lavi S, Shatkin AJ. Methylated simian virus 40-specific RNA from nuclei and cytoplasm of
597 infected BSC-1 cells. 1975;72: 2012–2016.

598 34. Krug RM, Morgan MA, Shatkin AJ. Influenza viral mRNA contains internal N(6)-
599 methyladenosine and 5'-terminal 7-methylguanosine in cap structures. J Virol. 1976;20:
600 45–53. doi:10.1177/1091581816683642

601 35. Kahana C, Lavi S, Groner Y. Identification and mapping of N(6)-methyladenosine
602 containing sequences in simian virus 40 RNA. Nucleic Acids Research. 1979;6: 2879–
603 2899.

604 36. Moss B, Gershowitz A, Stringer JR, Holland LE, Wagner EK. 5'-Terminal and internal
605 methylated nucleosides in herpes simplex virus type 1 mRNA. J Virol. 1977;23: 234–239.

606 37. Sommer S, Salditt-Georgieff M. The methylation of adenovirus-specific nuclear and
607 cytoplasmic RNA. Nucleic Acids Research. 1976;3: 749–765.

608 38. Ye F, Chen ER, Nilsen TW. Kaposi's Sarcoma-Associated Herpesvirus Utilizes and
609 Manipulates RNA N(6)-Adenosine Methylation To Promote Lytic Replication. J Virol.
610 2017;91. doi:10.1128/JVI.00466-17

611 39. Vieira J, O'Hearn PM. Use of the red fluorescent protein as a marker of Kaposi's sarcoma-
612 associated herpesvirus lytic gene expression. Virology. 2004;325: 225–240.
613 doi:10.1016/j.virol.2004.03.049

614 40. Myoung J, Ganem D. Infection of Lymphoblastoid Cell Lines by Kaposi's Sarcoma-

615 Associated Herpesvirus: Critical Role of Cell-Associated Virus. J Virol. 2011;85: 9767–
616 9777. doi:10.1128/JVI.05136-11

617 41. Dominissini D, Moshitch-Moshkovitz S, Schwartz S, Salmon-Divon M, Ungar L, Osenberg
618 S, et al. Topology of the human and mouse m6A RNA methylomes revealed by m6A-seq.
619 Nature. 2012;485: 201–206. doi:10.1038/nature11112

620 42. Sun R, Lin SF, Gradoville L, Miller G. Polyadenylylated nuclear RNA encoded by Kaposi
621 sarcoma-associated herpesvirus. PNAS. 1996;93: 11883–11888.

622 43. Bai Z, Huang Y, Li W, Zhu Y, Jung JU, Lu C, et al. Genomewide mapping and screening of
623 Kaposi's sarcoma-associated herpesvirus (KSHV) 3'untranslated regions identify
624 bicistronic and polycistronic viral transcripts as frequent targets of KSHV microRNAs. J
625 Virol. 2014;88: 377–392. doi:10.1128/JVI.02689-13

626 44. Chandriani S, Ganem D. Array-based transcript profiling and limiting-dilution reverse
627 transcription-PCR analysis identify additional latent genes in Kaposi's sarcoma-associated
628 herpesvirus. J Virol. 2010;84: 5565–5573. doi:10.1128/JVI.02723-09

629 45. Lukac DM, Kirshner JR, Ganem D. Transcriptional activation by the product of open
630 reading frame 50 of Kaposi's sarcoma-associated herpesvirus is required for lytic viral
631 reactivation in B cells. J Virol. 1999;73: 9348–9361.

632 46. Ke S, Pandya-Jones A, Saito Y, Fak JJ, Vågbø CB, Geula S, et al. m(6)A mRNA modifications
633 are deposited in nascent pre-mRNA and are not required for splicing but do specify
634 cytoplasmic turnover. Genes Dev. 2017;31: 990–1006. doi:10.1101/gad.301036.117

635 47. Cleary MD, Meiering CD, Jan E, Guymon R, Boothroyd JC. Biosynthetic labeling of RNA
636 with uracil phosphoribosyltransferase allows cell-specific microarray analysis of mRNA
637 synthesis and decay. Nat Biotechnol. 2005;23: 232–237. doi:10.1038/nbt1061

638 48. Woodford TA, Schlegel R, Pardee AB. Selective isolation of newly synthesized mammalian
639 mRNA after in vivo labeling with 4-thiouridine or 6-thioguanosine. Analytical
640 biochemistry. 1988;171: 166–172. doi:10.1016/0003-2697(88)90138-8

641 49. Nakamura H, Lu M, Gwack Y, Souvlis J, Zeichner SL, Jung JU. Global Changes in Kaposi's
642 Sarcoma-Associated Virus Gene Expression Patterns following Expression of a
643 Tetracycline-Inducible Rta Transactivator. J Virol. 2003;77: 4205–4220.
644 doi:10.1128/JVI.77.7.4205-4220.2003

645 50. Wang Y, Li Y, Toth JI, Petroski MD, Zhang Z, Zhao JC. N(6)-methyladenosine modification
646 destabilizes developmental regulators in embryonic stem cells. Nat Cell Biol. 2014;16:
647 191–198. doi:10.1038/ncb2902

648 51. Lin S, Choe J, Du P, Triboulet R, Gregory RI. The m(6)A Methyltransferase METTL3
649 Promotes Translation in Human Cancer Cells. Molecular Cell. 2016;62: 335–345.

650 doi:10.1016/j.molcel.2016.03.021

651 52. Wu R, Jiang D, Wang Y, Wang X. N(6)-Methyladenosine (m(6)A) Methylation in mRNA
652 with A Dynamic and Reversible Epigenetic Modification. Mol Biotechnol. 2016;58: 450–
653 459. doi:10.1007/s12033-016-9947-9

654 53. Fry NJ, Law BA, Ilkayeva OR, Holley CL, Mansfield KD. N(6)-methyladenosine is required
655 for the hypoxic stabilization of specific mRNAs. RNA. 2017;23: 1444–1455.
656 doi:10.1261/rna.061044.117

657 54. Davis ZH, Verschueren E, Jang GM, Kleffman K, Johnson JR, Park J, et al. Global mapping
658 of herpesvirus-host protein complexes reveals a transcription strategy for late genes.
659 Molecular Cell. 2015;57: 349–360. doi:10.1016/j.molcel.2014.11.026

660 55. Abernathy E, Gilbertson S, Alla R, Glaunsinger B. Viral Nucleases Induce an mRNA
661 Degradation- Transcription Feedback Loop in Mammalian Cells. Cell Host Microbe.
662 2015;18: 243–253. doi:10.1016/j.chom.2015.06.019

663 56. Dominissini D, Moshitch-Moshkovitz S, Salmon-Divon M, Amariglio N, Rechavi G.
664 Transcriptome-wide mapping of N(6)-methyladenosine by m(6)A-seq based on
665 immunocapturing and massively parallel sequencing. Nat Protoc. 2013;8: 176–189.
666 doi:10.1038/nprot.2012.148

667 57. Arias C, Weisburd B, Stern-Ginossar N, Mercier A, Madrid AS, Bellare P, et al. KSHV 2.0: a
668 comprehensive annotation of the Kaposi's sarcoma-associated herpesvirus genome using
669 next-generation sequencing reveals novel genomic and functional features. PLoS Pathog.
670 2014;10: e1003847. doi:10.1371/journal.ppat.1003847

671

672 **Figure Legends:**

673 **Fig 1. m^6A increases upon KSHV reactivation.** (A) Schematic of the experimental setup.
674 iSLK.219 cells were induced with doxycycline for 5 days to induce the lytic cycle, and total RNA
675 was collected and subjected to oligo dT selection to purify poly(A) RNA. Polyadenylated RNA
676 was spiked with 10uM of 5-fluorouridine and digested with nuclease P1 and alkaline
677 phosphatase, and subjected to LC-MS/MS analysis. (B) Relative m^6A content in iSLK.219 cells.
678 The induced sample was normalized with respect to the uninduced sample (set to 1).

679

680 **Fig 2. KSHV mRNA contains m^6A modifications.** (A) Two independent replicates of iSLK.219
681 cells containing latent KSHV were treated with dox for 5 days to induce the viral lytic cycle
682 (induced) or left untreated to preserve viral latency (uninduced). DNase-treated RNA was
683 isolated and subjected to m^6Aseq. Displayed are peaks with a fold change of four or higher,
684 comparing reads in the m^6A-IP to the corresponding input. (B) Overview of sequencing reads
685 from induced m^6A IP samples, aligned to the ORF50 transcript and the annotated GG(m^6A)C

686 consensus motifs found in exon 2 of ORF50. The red and green colored bars denote the
687 sequences encompassed by the FC>4 peaks in each replicate. (C) Cells were induced as in (A),
688 and total RNA was subjected to m^6A RIP, followed by RT-qPCR using primers for the indicated
689 viral and cellular genes. Values are displayed as fold change over input. (D) Quantification of
690 cellular m^6A peaks from m^6Aseq analysis.

691

692 **Fig 3. m^6A and the reader YTHDF2 potentiate viral gene expression and virion production in**
693 **iSLK.219 cells.** Cells were transfected with control scramble (scr) siRNAs or siRNAs against
694 Mettl3, YTHDF1, 2, or 3, then reactivated for 72 hours with doxycycline and sodium butyrate.
695 (A) Knockdown efficiency was measured by western blot using antibodies for the indicated
696 protein, with GAPDH serving as a loading control in this and all subsequent figures. (B) Viral
697 supernatant was collected from the reactivated iSLK.219 cells and transferred to uninfected
698 HEK293T recipient cells. 24 h later, the recipient cells were analyzed by flow cytometry for the
699 presence of GFP, indicating transfer of infectious virions. (C) ORF50, ORF37, ORF57, and K8.1
700 gene expression was analyzed by RT-qPCR from cells treated with the indicated siRNAs. One
701 representative experiment, matched to the siRNA knockdown in *(A)* is shown. (D) Expression of
702 the viral ORF50 and ORF59 proteins in cells treated with the indicated siRNAs was measured by
703 western blot 72hr post-reactivation. (E) Unreactivated iSLK.219 cells containing latent virus
704 were treated with control scramble (scr) siRNAs or siRNAs targeting Mettl3, YTHDF1, YTHDF2,
705 or YTHDF3. The cells were then reactivated with dox and sodium butyrate for 48 hr and lytic
706 reactivation was monitored by expression of the lytic promoter-driven red fluorescent protein.
707 (F) Protein was harvested from the above described cells and subjected to western blot for
708 ORF50 and the control GAPDH protein at 24 hr post-reactivation.

709

710 **Fig 4. Depletion of the m^6A writer and readers does not impact ORF50 nascent transcription**
711 **in iSLK.219 cells.** (A) Schematic of the experimental setup for measuring nascent RNA
712 synthesis. Cells were transfected with the indicated siRNAs for 48h then reactivated for 24
713 hours with dox. 4SU was added for 30 minutes, whereupon nascent 4SU-labeled RNA was
714 isolated using biotin/streptavidin affinity purification, reverse transcribed, and analyzed by RT-
715 qPCR using primers specific to ORF50 or ORF37. (B-C) Levels of nascent ORF50 *(B)* or ORF37
716 mRNA *(C)*, determined as described above. Unpaired Student's t test was used to evaluate the
717 statistical difference between samples. Significance was evaluated with P values <0.05. (D-E)
718 Uninfected iSLK.puro cells expressing DOX-inducible RTA were transfected with the indicated
719 siRNAs for 48 h, then treated with dox for 24 hours to induce ORF50 expression. Knockdown
720 efficiency *(D)* and ORF50 protein levels *(E)* were measured by western blot using antibodies for
721 the indicated protein, with GAPDH serving as a loading control.

722

723 **Fig 5. Increased viral gene expression upon m^6A writer and reader depletion in TREX-BCBL1**
724 **cells.** (A-B, D) TREX-BCBL1 cells were nucleofected with control scramble (scr) siRNAs or siRNAs
725 specific to Mettl3, YTHDF1, YTHDF2, or YTHDF3, then lytically reactivated by treatment with

726 dox, TPA and ionomycin for 72 hr. (A) Knockdown efficiency of the m^6A proteins relative to the
727 loading control GAPDH was quantified by western blot. (B) Levels of the KSHV ORF50 and
728 ORF59 proteins were assayed by western blot in the control and m^6A protein-depleted samples.
729 (C) TREX-BCBL1 cells were reactivated with dox for 72 hr, then total RNA was isolated and
730 subjected to m^6A RIP, followed by RT-qPCR for analysis of KSHV ORF50, GAPDH, and DICER.
731 Values are displayed as fold change over input. (D) Viral supernatant from the reactivated
732 control or m^6A protein depleted TREX-BCBL1 cells was transferred to uninfected HEK293T
733 recipient cells, whereupon transfer of infection was quantified by RT-qPCR for the viral LANA
734 transcript 48 hr post-supernatant transfer.

735

736

737 **Supporting Information:**

738 **S1. Fig. Location of union FC>4 peaks within KSHV transcriptome.** Overview of sequencing
739 reads aligned to regions of the KSHV transcriptome containing m^6A modifications. Depicted are
740 peaks with a fold change of four or higher in both replicates, comparing reads in the m^6A-IP to
741 the corresponding input. The blue and purple bars denote the sequences encompassed by the
742 FC>4 peaks in each uninduced replicate (A), while the red and green colored bars denote the
743 FC>4 peaks in each induced replicate (B). In the reference transcriptome, grey bars indicate
744 annotated 3'UTRs or ncRNAs, while burgundy arrows depict ORFs. Note that the alignment of
745 the ORF50 induced peaks can be found in Figure 2.

746

747 S1. Table: Full list of FC>2 peaks within KSHV transcripts in induced and uninduced samples.

748 S2. Table: Full list of FC>4 peaks within host transcripts in induced and uninduced samples.

749 S3. Table: List of RT-qPCR primers used in this study.

Primer	Sequence (5'-3')	Orientation F: Forward R: Reverse
vIL6	CGGTTCACTGCTGGTATCTG	F
vIL6	CAGTATCGTTGATGGCTGGT	R

ORF57	TTTGACGAATCGAGGGACGACG	F
ORF57	GCAGTTGAGAACGACCTTGAGAT	R
ORF37	TGGGCGAGTTTATTGGTAGTGAGG	F
ORF37	CTCCACTAGACAGCAGATGTGG	R
K8.1	TCCCTAAACGGGACCAGACT	F
K8.1	ACCCAGAGGCAGACGTATCT	R
PAN	TAATGTGAAAGGAAAGCAGCGCCC	F
PAN	CATTTAGGGCAAAGTGGCCCGATT	R
vGPCR	GTGCCTTACACGTGGAACGTT	F
vGPCR	GGTGACCAATCCATTTCCAAGA	R
K1	CCAAACGGACGAAATGAAAC	F
K1	TGTGTGGTTGCATCGCTATT	R
GAPDH	CGGAGTCAACGGATTTGGTCGTAT	F
GAPDH	AGCCTTCTCCATGGTGGTGAAGAC	R
ORF50	CGCAATGCGTTACGTTGTTG	F
ORF50	GCCCGGACTGTTGAATCG	R
DICER	TGCTATGTCGCCTTGAATGTT	F

DICER	AATTTCTCGATAGGGGTGGTCTA	R
18s	GTAACCCGTTGAACCCCATT	F
18s	CCATCCAATCGGTAGTAGCG	R
LANA	TGGCCCATCTCGCGAATA	F
LANA	AACGCGCCTCATACGAACTC	R

750

A

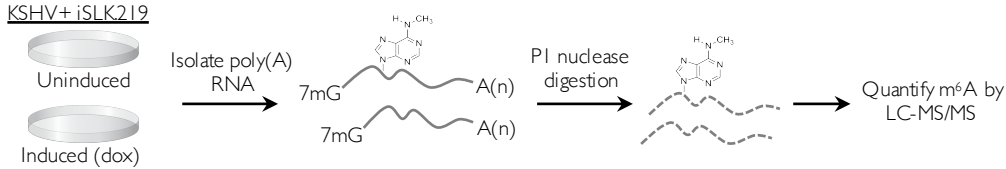
KSHV+ iSLK.219
Uninduced
Induced (dox)
Isolate poly(A) RNA
7mG
A(n)
7mG
A(n)
P1 nuclease digestion
Quantify m6A by LC-MS/MS

B

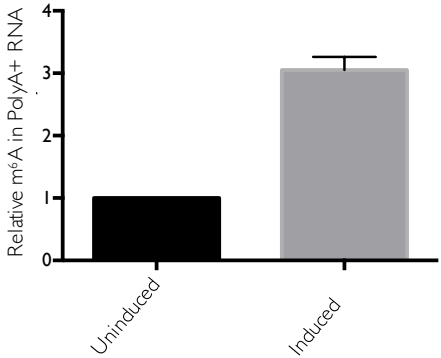
Total m6A levels by MS/MS
Relative m6A in PolyA+ RNA
4
3
2
1
0
Uninduced
Induced

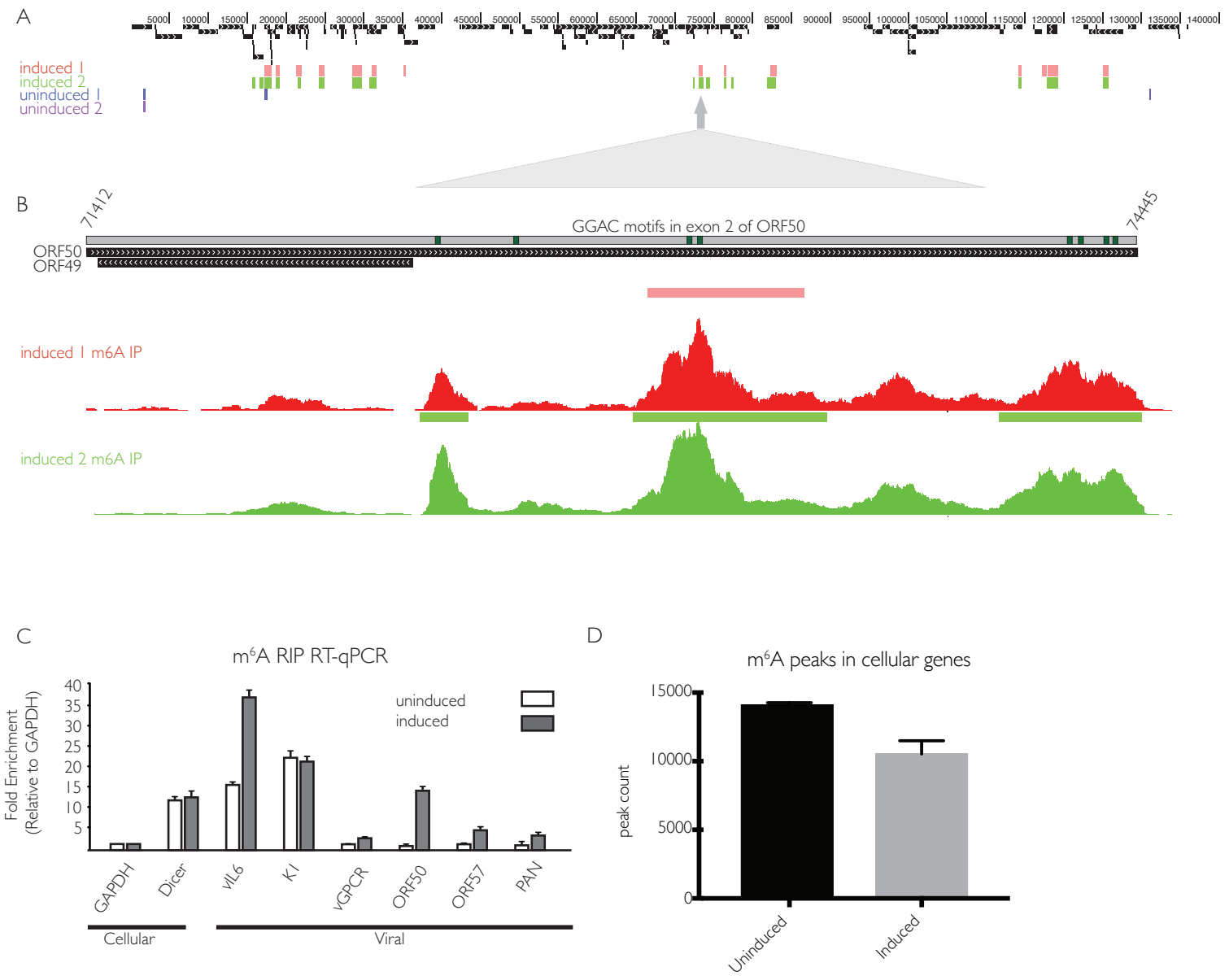
A
5000
10000
15000
20000
25000
30000
35000
40000
45000
50000
55000
60000
65000
70000
75000
80000
85000
90000
95000
100000
105000
110000
115000
120000
125000
130000
135000
140000
induced 1
induced 2
uninduced 1
uninduced 2
B
71412
74445
GGAC motifs in exon 2 of ORF50
ORF50
ORF49
induced 1 m6A IP
induced 2 m6A IP
C
m6A RIP RT-qPCR
Fold Enrichment
(Relative to GAPDH)
40
35
30
25
20
15
10
5
uninduced
induced
GAPDH
Dicer
vIL6
K1
vGPCR
ORF50
ORF57
PAN
Cellular
Viral
D
m6A peaks in cellular genes
peak count
15000
10000
5000
0
Uninduced
Induced

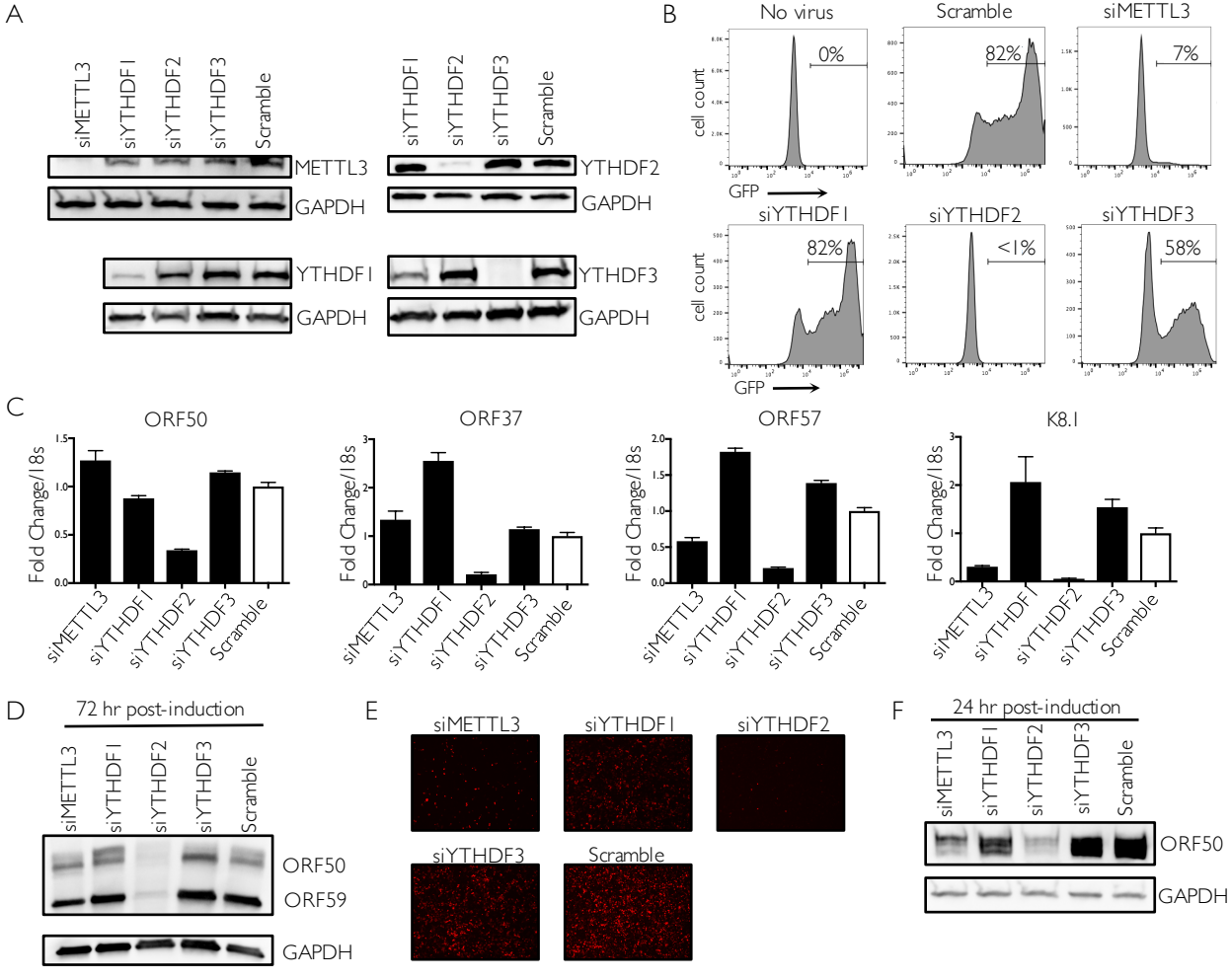
A
siMETTL3
siYTHDF1
siYTHDF2
siYTHDF3
Scramble
METTL3
GAPDH
YTHDF2
YTHDF1
YTHDF3
B
No virus
Scramble
siMETTL3
siYTHDF1
siYTHDF2
siYTHDF3
0%
82%
7%
82%
<1%
58%
cell count
GFP
C
ORF50
ORF37
ORF57
K8.1
Fold Change/18s
D
72 hr post-induction
ORF50
ORF59
E
F
24 hr post-induction

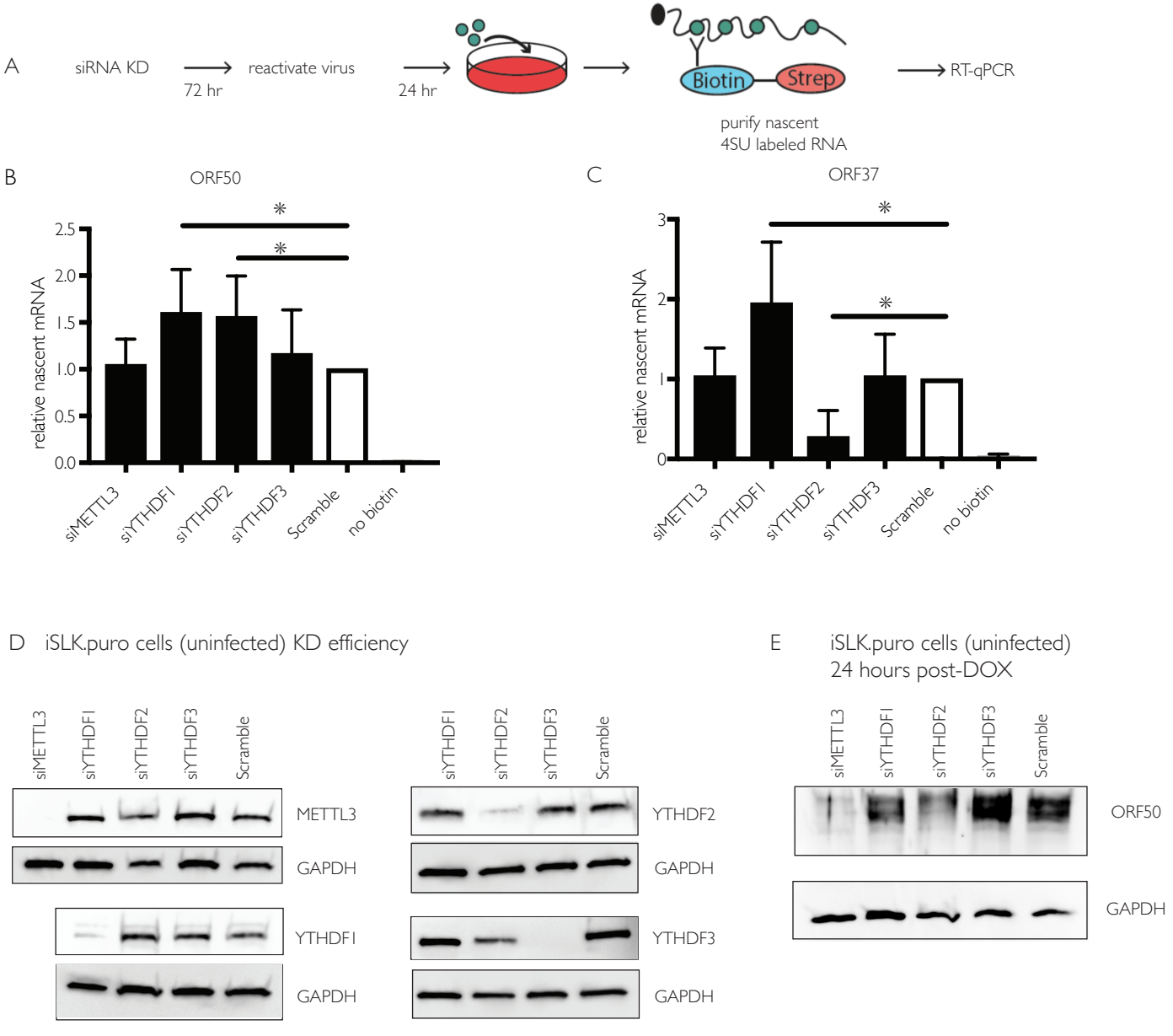
A
siRNA KD
72 hr
reactivate virus
24 hr
Biotin
Strep
purify nascent
4SU labeled RNA
RT-qPCR
B
ORF50
relative nascent mRNA
2.5
2.0
1.5
1.0
0.5
0.0
*
*
siMETTL3
siYTHDF1
siYTHDF2
siYTHDF3
Scramble
no biotin
C
ORF37
relative nascent mRNA
3
2
1
0
*
*
siMETTL3
siYTHDF1
siYTHDF2
siYTHDF3
Scramble
no biotin
D iSLK.puro cells (uninfected) KD efficiency
siMETTL3
siYTHDF1
siYTHDF2
siYTHDF3
Scramble
METTL3
GAPDH
YTHDF1
GAPDH
siYTHDF1
siYTHDF2
siYTHDF3
Scramble
YTHDF2
GAPDH
YTHDF3
GAPDH
E iSLK.puro cells (uninfected)
24 hours post-DOX
siMETTL3
siYTHDF1
siYTHDF2
siYTHDF3
Scramble
ORF50
GAPDH

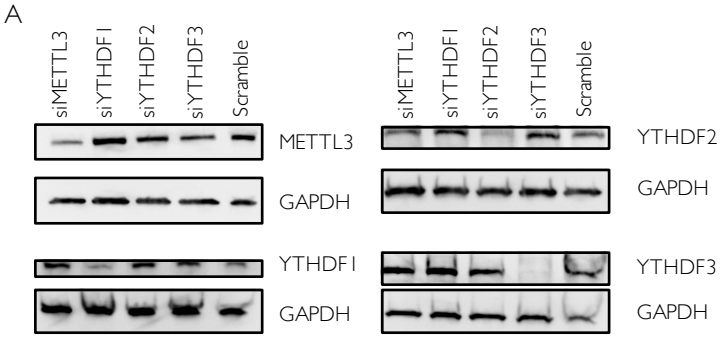
A
siMETTL3
siYTHDF1
siYTHDF2
siYTHDF3
Scramble
METTL3
GAPDH
YTHDF1
GAPDH
YTHDF2
GAPDH
YTHDF3
GAPDH

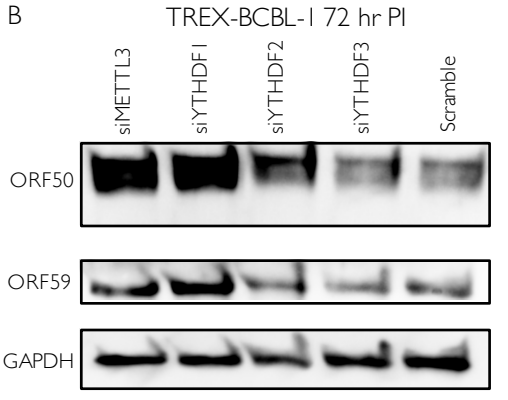
B
TREX-BCBL-1 72 hr PI
siMETTL3
siYTHDF1
siYTHDF2
siYTHDF3
Scramble
ORF50
ORF59
GAPDH

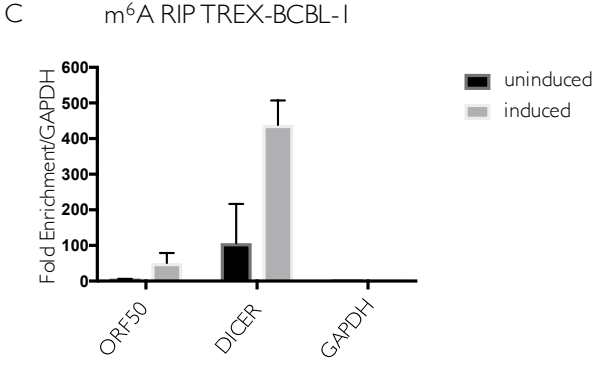
C
m6A RIP TREX-BCBL-1
Fold Enrichment/GAPDH
600
500
400
300
200
100
0
uninduced
induced
ORF50
DICER
GAPDH

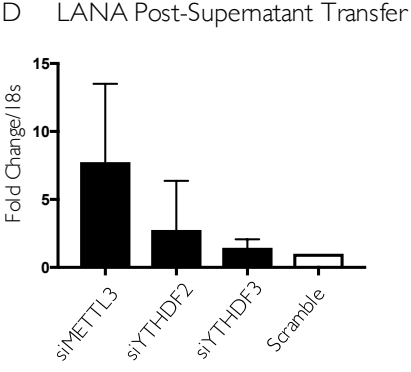
D
LANA Post-Supernatant Transfer
Fold Change/18s
15
10
5
0
siMETTL3
siYTHDF2
siYTHDF3
Scramble